Hydrol. Earth Syst. Sci. Discuss., 12, 7821–7842, 2015
www.hydrol-earth-syst-sci-discuss.net/12/7821/2015/
doi:10.5194/hessd-12-7821-2015

Hydrology and Earth System Sciences
Open Access
Discussions

Does the Budyko curve reflect a maximum power state of hydrological systems? A backward analysis

M. Westhoff[1], **E. Zehe**[2], **P. Archambeau**[1], **and B. Dewals**[1]

[1]Hydraulics in Environmental and Civil Engineering (HECE), University of Liege (ULg), Liege, Belgium
[2]Karlsruhe Institute of Technology (KIT), Karlsruhe, Germany

Received: 23 July 2015 – Accepted: 27 July 2015 – Published: 11 August 2015

Correspondence to: M. Westhoff (martijn.westhoff@ulg.ac.be)

Published by Copernicus Publications on behalf of the European Geosciences Union.

Abstract

Almost all catchments plot within a small envelope around the Budyko curve. This apparent behaviour suggests that organizing principles may play a role in the evolution of catchments. In this paper we applied the thermodynamic principle of maximum power as the organizing principle.

In a top-down approach we derived mathematical formulations of the relation between relative wetness and gradients driving runoff and evaporation for a simple one-box model. We did this in such a way that when the conductances are optimized with the maximum power principle, the steady state behaviour of the model leads exactly to a point on the Budyko curve. Subsequently we derived gradients that, under constant forcing, resulted in a Budyko curve following the asymptotes closely. With these gradients we explored the sensitivity of dry spells and dynamics in actual evaporation. Despite the simplicity of the model, catchment observations compare reasonably well with the Budyko curves derived with dynamics in rainfall and evaporation. This indicates that the maximum power principle may be used (i) to derive the Budyko curve and (ii) to move away from the empiricism in free parameters present in many Budyko functions. Future work should focus on better representing the boundary conditions of real catchments and eventually adding more complexity to the model.

1 Introduction

In different climates, partitioning of rainwater into evaporation and runoff is different as well. Yet, when plotting the evaporation fraction against the aridity index (ratio of potential evaporation and rainfall), almost all catchments plot in a small envelope around a single empirical curve known as the Budyko curve (e.g. Arora, 2002). The fact that almost all catchments worldwide plot within this small envelope around this curve inspired several scientists to speculate whether this is due to co-evolution of climate and terrestrial catchment characteristics (e.g. Harman and Troch, 2014). Co-evolution be-

HESSD
12, 7821–7842, 2015

tween climate and the terrestrial system could in turn be explained by an underlying organizing principle which determines optimum system functioning (Sivapalan et al., 2003; McDonnell et al., 2007; Schaefli et al., 2011; Thompson et al., 2011; Ehret et al., 2014; Zehe et al., 2014). As hydrological processes are essentially dissipative, we suggest that thermodynamic optimality principles are very interesting candidates.

Belonging to this class of principles are the closely related principles of maximum entropy production (Kleidon and Schymanski, 2008; Kleidon, 2009; Porada et al., 2011; Wang and Bras, 2011; del Jesus et al., 2012; Westhoff and Zehe, 2013) and maximum power (Kleidon and Renner, 2013; Kleidon et al., 2013; Westhoff et al., 2014) on the one hand – both defining the optimum configuration between competing fluxes across the system boundary – and, on the other hand, minimum energy dissipation (Rinaldo et al., 1992; Rodriguez-Iturbe et al., 1992; Hergarten et al., 2014) or maximum free energy dissipation (Zehe et al., 2010, 2013), focusing on free energy dissipation associated with changes in internal state variables as a result of boundary fluxes, i.e. soil moisture and capillary potential, and a related optimum system configuration. In this research we focus on the maximum power principle.

With these principles, an optimum configuration between two competing fluxes can be determined. It seems therefore potentially suitable to derive the Budyko curve from such a principle, since the Budyko curve describes the competition between runoff and evaporation. This is also the aim of this study.

The validity and the practical value of thermodynamic optimality principles are still debated and the partly promising results reported in the listed studies might be just a matter of coincidence. There is a vital search for defining rigorous tests to assess how far thermodynamic optimality principles bears and applies. The Budyko curve appears very well suited for such a test, as it condenses relative weights of the steady state water fluxes in most catchments around the world. It is thus not astonishing that there have been several attempts to reconcile the Budyko curve with thermodynamic optimality principles. For example, Porada et al. (2011) used the maximum entropy production principle to optimize the runoff conductance and evaporation conductance

HESSD
12, 7821–7842, 2015

of a bucket model being forced with observed rainfall and potential evaporation of the 35 largest catchments in the world. The resulting modelled fluxes were plotted in the Budyko diagram and followed the curve with a similar scatter as real world catchments.

Another very interesting approach was presented by Kleidon and Renner (2013) and Kleidon et al. (2014), using the perspective of the atmosphere. They maximized power of the vertical convective motion transporting heat and moisture upwards using the Carnot limit to constrain the sensible heat flux. This motion is driven by the temperature differences between the surface and the atmosphere, while at the same time depleting this temperature gradient, leading to a maximum in power. Additionally, evaporation at the surface and condensation in the atmosphere depletes this gradient even further at the expense of more vertical moisture transport and thus more convective motion. Their approach showed some more spreading around the Budyko curve for the same 35 catchments as used in Porada et al. (2011), but they used a simpler model that has to be forced with much less observations, namely solar radiation, precipitation and surface temperature.

Very recently, Wang et al. (2015) used the maximum entropy production principle to derive directly an expression for the Budyko curve. They started from the expression of Kleidon and Schymanski (2008) and by maximizing the entropy production of the whole system they reached the expression for the Budyko curve as formulated by Wang and Tang (2014). This is an intriguing result that partly contradicts the findings of Westhoff and Zehe (2013), whose study revealed within simulations with an HBV type conceptual model, that joint optimization of overall entropy production results in optimum conductances approaching zero.

In this study we used a model comparable to the one proposed by Porada et al. (2011) and derived the Budyko curve from the maximum power hypothesis in an inverse manner. With this backward analysis we found proper relations between relative saturation of the subsurface and the gradients driving runoff and evaporation.

This backward analysis is performed for constant forcing and evaporation. Since Westhoff et al. (2014) showed mathematically that dynamics in forcing or in actual

HESSD
12, 7821–7842, 2015

evaporation may result to different optimum conductances (and sometimes even two maxima in power) we tested sensitivities to these dynamics here as well. We expect these dynamics to influence the optimum conductance k_e^* and subsequently the whole Budyko curve.

2 The maximum power principle

The maximum power principle implies that a system evolves in such a way that steady state fluxes across a systems boundary produce maximum power. It is directly derived from the first and the second laws of thermodynamics, and is very well explained in Kleidon and Renner (e.g. 2013). Here we give only a short description: let us start by considering a warm and a cold reservoir, which are connected to each other. The warm reservoir is forced by a constant energy input J_{in} and the cold reservoir is cooled by a heat flux J_{out}. In steady state $J_{in} = J_{out}$ and both reservoirs have a constant temperature T_h and T_c, respectively, with $T_h > T_c$. The heat flux between the two reservoirs produces entropy, which is given by:

$$\sigma = \frac{J_{out}}{T_c} - \frac{J_{in}}{T_h}. \quad (1)$$

However, instead of transferring all incoming energy to the cold reservoir, the heat gradient can also be used to perform work. This means that in steady state, the incoming energy flux J_{in} equals the outgoing energy flux J_{out} plus the rate of work P (which is power) performed by the system.

For given temperatures of both reservoirs, the theoretical maximum rate of work is given by the Carnot limit:

$$P_{Carnot} = J_{in} \frac{T_h - T_c}{T_h}. \quad (2)$$

HESSD
12, 7821–7842, 2015

Power is thus given as the product of a flux (in this case J_{in}) and its driving potential difference (in this case $(T_h - T_c)$ scaled by T_h). Since the temperature of both reservoirs is also influenced by the heat flux between the two reservoirs, there exist a trade-off between the flux and the temperature difference. Subsequently, a maximum in power exists.

In the remainder of this article we used specific water fluxes [LT^{-1}] and potential differences $\mu_{high} - \mu_{low}$ in meter water column [L], where the flux is given as the product of a specific conductance k [T^{-1}] and the potential difference. We recognize that, in order to come to the same units as power, these formulations should be multiplied by the water density, gravitational acceleration and a cross-sectional area, but since we are looking for a maximum, and these parameters are constant, we can leave them out. We also use the word gradient for the potential difference $\mu_{high} - \mu_{low}$, where the length scale with which the difference should be divided is incorporated in the conductance. With these formulation, power is given by

$$P = k\left(\mu_{high} - \mu_{low}\right)^2 \quad (3)$$

where k is the free parameter we optimized to find a maximum in power.

3 Mathematical framework

3.1 Initial model setup

Our model consists of a simple reservoir being filled by rainfall Q_{in} and drained by evaporation E_a and runoff Q_r. Using the same expressions as in Kleidon and Schymanski (2008), the steady state mass balance and corresponding fluxes are expressed by

$$Q_{in} = E_a + Q_r \quad (4)$$

$$E_a = k_e\left(\mu_s - \mu_{atm}\right) \quad (5)$$

$$Q_r = k_r\left(\mu_s - \mu_r\right) \quad (6)$$

HESSD
12, 7821–7842, 2015

where μ_s, μ_r and μ_{atm} are the chemical potential of the soil, chemical potential of the free water surface of the nearest river and chemical potential of the atmosphere, while k_e and k_r are the specific conductances of evaporation and runoff. In these expressions, μ_s and $\mu_s - \mu_r$ are functions of the relative saturation h in the reservoir:

$$G_e(h) = \mu_s(h) \quad (7)$$

$$G_r(h) = \mu_s(h) - \mu_r(h) \quad (8)$$

where $G_e(h)$ and $G_r(h)$ can have any form as long as they are strictly monotonically increasing with increasing relative saturation. For example, Porada et al. (2011) used the van Genuchten model (van Genuchten, 1980) and gravitational potential to derive the chemical potential of the soil. However, here we will derive them in such a way that, under constant forcing, we end up exactly at the Budyko curve.

3.2 Backwards analysis to determine the driving gradients

3.2.1 Optimum k_e^* matching the Budyko curve

Let us first find an optimum conductance k_e^* leading to a point on the Budyko curve. We started with the following expression for the Budyko curve (e.g. Choudhury, 1999; Yang et al., 2008, although other expression can in principle be used as well):

$$\frac{E_a}{Q_{in}} = \frac{1}{\left(1 + \frac{Q_{in}^n}{E_{pot}^n}\right)^{1/n}} \quad (9)$$

with E_{pot} being the potential evaporation. Now we make an important assumption to define E_{pot}: we assume that evaporation is maximum when in Eqs. (5) and (8), $\mu_s = 0$, meaning that the relative wetness is 1, implying no water limitation. With this assumption, potential evaporation is given by $E_{pot} = k_e^*(-\mu_{atm})$ (note that μ_{atm} is always negative). Combining this equation with Eqs. (5), (7) and (9) results in:

HESSD
12, 7821–7842, 2015

$$k_e^* = \frac{Q_{in}}{(G_e(h^*) - \mu_{atm})\left(1 + \left[\frac{Q_{in}}{-k_e^* \mu_{atm}}\right]^n\right)^{1/n}} \quad (10)$$

where h^* is the steady state relative wetness leading to a point at the Budyko curve.

3.2.2 Maximum power by evaporation

As mentioned above, k_e^* should also correspond to a maximum in power by evaporation (P_e). This means that a function $P_e(k_e)$ should be found which is always larger than zero for $k_e \in (0, +\infty)$ and where $\partial P_e / \partial k_e = 0$ at $k_e = k_e^*$. A possible function satisfying these constraints is:

$$P_e(k_e) = k_e \frac{P_0}{k_0} e^{-\left(\frac{k_e - a}{k_0}\right)^2} \quad (11)$$

where P_0 and k_0 are the reference power [L^2T^{-1}] and reference conductance [T^{-1}], respectively. Setting the derivative to zero for $k_e = k_e^*$ yields:

$$\frac{\partial P_e}{\partial k_e} = \left(2k_e^* a - 2k_e^{*2} + k_0^2\right) \frac{P_0}{k_0^3} e^{-\left(\frac{k_e^* - a}{k_0}\right)^2} = 0 \quad (12)$$

$$\rightarrow a = k_e^* - \frac{k_0^2}{2k_e^*}$$

resulting in $P_e(k_e) = k_e P_0 / k_0 e^{-\left((k_e - k_e^*)/k_0 + k_0/(2k_e^*)\right)^2}$.

Combining this expression with Eqs. (3) and (7): $P_e = k_e (G_e - \mu_{atm})^2$, G_e is expressed as:

$$G_e(k_e) = \pm \sqrt{\frac{P_0}{k_0} e^{-\left(\frac{k_e - k_e^*}{k_0} + \frac{k_0}{2k_e^*}\right)^2}} + \mu_{atm}. \quad (13)$$

HESSD
12, 7821–7842, 2015

Since we neglect condensation ($G_e(k_e) - \mu_{atm} \geq 0$), only the positive solution remains. Inserting Eq. (13) into Eq. (10) and setting $k_e = k_e^*$ yields:

$$k_e^* = \frac{Q_{in}}{\sqrt{\frac{P_0}{k_0} e^{-\frac{k_0^2}{4k_e^{*2}}}} \left(1 + \left[\frac{Q_{in}}{-k_e^* \mu_{atm}}\right]^n\right)^{1/n}} \tag{14}$$

which can be solved iteratively for k_e^*.

Combining these results with the mass balance (Eqs. 4–6) yields the following expression for runoff gradient G_r as a function of k_e:

$$G_r(k_e) = \frac{Q_{in}}{k_r} - \frac{k_e}{k_r} \sqrt{\frac{P_0}{k_0} e^{-\left(\frac{k_e - k_e^*}{k_0} + \frac{k_0}{2k_e^*}\right)^2}}. \tag{15}$$

Note that any value of k_r does lead to a point on the Budyko curve.

3.2.3 Maximum power by runoff

Although the Budyko curve does not depend on the value of k_r, an optimum k_r^* can still be found by maximizing power by runoff. For this, the similar steps as for optimizing k_e are used, where in Eqs. (11)–(13) k_e is simply replaced by k_r, resulting in a gradient for runoff as a function of k_r:

$$G_r(k_r) = \sqrt{\frac{P_0}{k_0} e^{-\left(\frac{k_r - k_r^*}{k_0} + \frac{k_0}{2k_r^*}\right)^2}} \tag{16}$$

while from the mass balance (Eqs. 4–8), k_r is given by

$$k_r = \frac{Q_{in} - [G_e(h) - \mu_{atm}]}{G_r(h)}. \tag{17}$$

HESSD
12, 7821–7842, 2015

Combining these two equations and setting k_r to k_r^* yields:

$$k_r^* = \frac{Q_{in} - k_e^* \left[G_e(k_e^*) - \mu_{atm}\right]}{\sqrt{\frac{P_0}{k_0} e^{-\frac{k_0^2}{4k_r^{*2}}}}} \quad (18)$$

which can also be solved iteratively for k_r^*.

3.3 Forward analysis

To apply the maximum power principle in any hydrological model, the model should run until a (quasi-)steady state is reached. Within the above presented backward analysis the steady state optimum gradients are simply found by giving k_e the value of k_e^* in Eq. (13) and $k_r = k_r^*$ in Eq. (15).

However, when the relative wetness h evolves over time, the gradients should be resolved as a function of the relative wetness ($G_e = G_e(h)$ and $G_r = G_r(h)$). To do this, we assumed that h is a linear function of $G_r(k_e)$ scaled between zero and unity:

$$G_r(h) = \min\left[G_r(k_e)\right] + \left(\max\left[G_r(k_e)\right] - \min\left[G_r(k_e)\right]\right) h \quad (19)$$

where the maximum in $G_r(k_e)$ occurs when the second term on the right-hand-side of Eq. (15) is zero: $\max\left[G_r(k_e)\right] = \frac{Q_{in}}{k_r}$ and the minimum value is derived when this second term is maximum, occurring at $k_e = k_e^{max} = 1/2\left(k_e^* - \frac{k_0^2}{2k_e^*} + \sqrt{\left(k_e^* - \frac{k_0^2}{2k_e^*}\right)^2 + 4}\right)$.

Inserting this into Eq. (15) yields:

$$\min\left[G_r(k_e)\right] = \frac{Q_{in}}{k_r} - \frac{k_e^{max}}{k_r}\sqrt{\frac{P_0}{k_0} e^{-\left(\frac{k_e^{max} - k_e^*}{k_0} + \frac{k_0}{2k_e^*}\right)^2}}. \quad (20)$$

HESSD
12, 7821–7842, 2015

If we now plot h vs. G_e, a unique relation between the two exists (Fig. 1).

With the gradients as functions of h, the non-steady mass balance equation is written as

$$S_{max}\frac{dh}{dt} = Q_{in} - k_r G_r(h) - k_e\left(G_e(h) - \mu_{atm}\right) \quad (21)$$

where S_{max} is the maximum storage depth [L] and t is time [T]. Now, the time evolution of the relative wetness can be simulated.

4 Results and discussion from forward analysis

4.1 Constant forcing

With the known relations between relative wetness and gradients driving evaporation and runoff, the forward model was run and k_e be optimized by maximizing power. With constant forcing, each value of μ_{atm} resulted in a point on the Budyko curve (Fig. 2a, a value of $n = 2$ is used). In Fig. 2b, the time evolution of the relative wetness and both gradients are shown for an initially saturated and an initially dry state indicating that irrespective of the initial state, the forward model evolves to a steady state.

4.2 Sensitivity to dry spells

By introducing dynamics in forcing, we expected the resulting budyko curve to deviate from the initial one derived with constant forcing. It therefore matters how the initial one looks like. The parameter n in Eq. (9) is the key parameter to adapt the initial curve.

In literature, a value of $n = 2$ (and small variations around) is often used since it gives a good fit for many catchments: In fact, n is an empirical parameter often linked to catchment properties. To move away from this empiricism for n, we subsequently used a much larger value in order to closely follow the asymptotes of the Budyko curve. A value of $n \longrightarrow +\infty$ follows these asymptotes exactly, but for numerical reasons we

HESSD
12, 7821–7842, 2015

used $n = 20$ (differences with $n = 10$ are minor (not shown)). Next, we added dry spells and dynamics in evaporation (e.g. when trees lose their leaves the evaporative conductance k_e goes to zero) and tested how this influenced the Budyko curve.

To test sensitivities to dry spells, simple block functions were used, with either a predefined constant input or no input at all. For longer relative lengths of the dry spell, the slope of the curves becomes smaller until a maximum of $E_a/Q_{in} = 0.98$ (Fig. 3). The reason the asymptotes do not reach unity lies in the fact that already at very short dry spells a second maximum in power evolves, while the first maximum disappears quickly with increasing dry spells. This is in line with results of Westhoff et al. (2014) while also in Zehe et al. (2013) a second optimum is present. Although interesting, we leave a better exploration of this transition zone where two maxima exist for future research.

These curves were compared with data of real catchments that have a relatively stable wet period interspersed with a regular dry period. The Mupfure catchment (Zimbabwe, Savenije, 2004) with approximately seven months without rain (Fig. S1 in the Supplement), plots very close to the theoretical curve with the same length of the dry spell. However, catchments from the MOPEX database (Schaake et al., 2006) with clear consistent dry spells plot still far from the respective theoretical curves. This discrepancy can be partly explained by the somewhat arbitrary way the number of dry months are determined: The MOPEX catchments are filtered to have only those catchments having at least one month with a median rainfall $< 2.5\,\mathrm{mm\,month^{-1}}$ and a coefficient of variance < 0.5 for all months with a median rainfall $> 25\,\mathrm{mm\,month^{-1}}$. The final number of dry months were determined maximizing the difference between the mean monthly precipitation of the X driest months minus the mean monthly precipitation of the $1 - X$ wettest months, where $X = 1, 2 \ldots 12$.

For example, the MOPEX catchment with a four month dry spell could also be argued to have a dry spell of seven months (Fig. S1, MOPEX ID: 11222000) and similarly, the MOPEX catchment with a five month dry spell (Fig. S1, MOPEX ID: 11210500) could also be argued to have one of six months. If these "corrections" are made, the variability

HESSD
12, 7821–7842, 2015

within the MOPEX catchments is consistent (with longer dry spells plotting more to the right), but there is still a discrepancy of one to two months, indicating that the model should still be improved.

4.3 Sensitivity to dynamics in actual evaporation

We also tested the sensitivity of dynamics in actual evaporation by periodically turning k_e on and off, while keeping the rainfall constant. This sensitivity analysis shows that the longer actual evaporation is switched off, the smaller the slope of the Budyko curve and the smaller the maximum value of the evaporation index (Fig. 4). Comparing the different curves with real catchments, shows that data from the Ourthe catchment (Belgium) is relatively close to its respective line (its months without actual evaporation are estimated from Fig. 6.1 of Aalbers, 2015). Also the MOPEX catchments plot relatively close to their respective lines. However, the way the MOPEX catchments were filtered is somewhat arbitrary (only those having a coefficient of variance < 0.12 for monthly median rainfall and with at least one month with a monthly median maximum ambient temperature $< 0\,^{\circ}\mathrm{C}$ are taken into account; a month is considered to have no actual evaporation if the monthly median maximum air temperature $< 0\,^{\circ}\mathrm{C}$; after Devlin, 1975, Fig. S2).

At first sight the comparison with data looks better than in the case of dry spells. However, all plotted catchments have an aridity index between 0.5 and 0.71 and within this range the different curves plot also close to each other. Yet, it is still somewhat surprising that the comparison is relatively good, since the modelled lines have been created by assuming a constant atmospheric demand (μ_{atm}) for each run, which is different from real catchments that have a more or less sinus shape potential evaporation over the year. However, we consider it as future work to better represent the real world dynamics in the model.

HESSD
12, 7821–7842, 2015

5 Conclusions and outlook

The Budyko curve is an empirical proof that only a subset of all possible combinations of aridity index and evaporation index emerges in nature. It belongs to the, so-called Darwinian models (Harman and Troch, 2014), focusing on emergent behaviour of a system as a whole. Since the maximum power principle links Newtonian models with the Darwinian models, it has indeed potential to derive the Budyko curve with an, in essence, Newtonian model.

We presented a top-down approach in which we derived relations between relative wetness and chemical potentials that lead, under constant forcing, to a point on the Budyko curve when the maximum power principle is applied. Subsequently sensitivities to dynamics in forcing and actual evaporation were tested.

Since the Budyko curve is an empirical curve, the parameter n is often linked to catchment specific characteristics such as land use, soil water storage, climate seasonality or spatial scales (e.g. Milly, 1994; Choudhury, 1999; Zhang et al., 2004; Potter et al., 2005). Although correlations between characteristics and n have been found, it remains a calibration parameter.

Here, to avoid an arbitrary (calibrated) value for n we used a large n, reflecting the two asymptotes of the Budyko curve, and analysed deviations from this line by introducing temporal dynamics. Although we used simple block functions to test these sensitivities they compare reasonably well with observations. Nevertheless, improvements could be made by modelling dynamics closer to reality, or even by adding multiple parallel reservoirs to account for spatial variability within a catchment.

Even though the model represents observations reasonably well (despite its simplicity), the method used here is by no means a proof that the maximum power principle does apply for hydrological systems. This is due to the top-down derivation of the gradients in which the maximum power principle is used explicitly. In principle, the method could also be used with respect to any other optimization principle. However, the rea-

HESSD
12, 7821–7842, 2015

sonable fits with observations gives floor to further explore this methodology – including the maximum power principle.

The Supplement related to this article is available online at doi:10.5194/hessd-12-7821-2015-supplement.

Acknowledgements. We would like to thank Miriam Coenders-Gerrits for providing data of the Mupfure catchment, Wouter Berghuis for his help with the MOPEX dataset and Service Public de Wallonie for providing river flow data of the Ourthe catchment. This research was supported by the University of Liege and the EU in the context of the MSCA-COFUND-BeIPD project.

References

Aalbers, E.: Evaporation in conceptual rainfall-runoff models: testing model realism using remotely sensed evaporation, Master's thesis, Delft University of Technology, available at: http://repository.tudelft.nl/view/ir/uuid:a2edc688-2270-4823-aa93-cb861cf481a2/, last access: 10 August 2015. 7833

Arora, V. K.: The use of the aridity index to assess climate change effect on annual runoff, J. Hydrol., 265, 164–177, doi:10.1016/S0022-1694(02)00101-4, 2002. 7822

Choudhury, B.: Evaluation of an empirical equation for annual evaporation using field observations and results from a biophysical model, J. Hydrol., 216, 99–110, doi:10.1016/S0022-1694(98)00293-5, 1999. 7827, 7834

del Jesus, M., Foti, R., Rinaldo, A., and Rodriguez-Iturbe, I.: Maximum entropy production, carbon assimilation, and the spatial organization of vegetation in river basins, P. Natl. Acad. Sci. USA, 109, 20837–20841, doi:10.1073/pnas.1218636109, 2012. 7823

Devlin, R.: Plant Physiology, 3rd Edn., D. Van Nostrand Company, New York, 1975. 7833, 7842

Ehret, U., Gupta, H. V., Sivapalan, M., Weijs, S. V., Schymanski, S. J., Blöschl, G., Gelfan, A. N., Harman, C., Kleidon, A., Bogaard, T. A., Wang, D., Wagener, T., Scherer, U., Zehe, E., Bierkens, M. F. P., Di Baldassarre, G., Parajka, J., van Beek, L. P. H., van Griensven, A., Westhoff, M. C., and Winsemius, H. C.: Advancing catchment hydrology to deal with predic-

HESSD

12, 7821–7842, 2015

tions under change, Hydrol. Earth Syst. Sci., 18, 649–671, doi:10.5194/hess-18-649-2014, 2014. 7823
Harman, C. and Troch, P. A.: What makes Darwinian hydrology "Darwinian"" Asking a different kind of question about landscapes, Hydrol. Earth Syst. Sci., 18, 417–433, doi:10.5194/hess-18-417-2014, 2014. 7822, 7834
Hergarten, S., Winkler, G., and Birk, S.: Transferring the concept of minimum energy dissipation from river networks to subsurface flow patterns, Hydrol. Earth Syst. Sci., 18, 4277–4288, doi:10.5194/hess-18-4277-2014, 2014. 7823
Kleidon, A.: Nonequilibrium thermodynamics and maximum entropy production in the Earth system, Naturwissenschaften, 96, 653–677, doi:10.1007/s00114-009-0509-x, 2009. 7823
Kleidon, A. and Renner, M.: Thermodynamic limits of hydrologic cycling within the Earth system: concepts, estimates and implications, Hydrol. Earth Syst. Sci., 17, 2873–2892, doi:10.5194/hess-17-2873-2013, 2013. 7823, 7824, 7825
Kleidon, A. and Schymanski, S.: Thermodynamics and optimality of the water budget on land: a review, Geophys. Res. Lett., 35, L20404, doi:10.1029/2008GL035393, 2008. 7823, 7824, 7826
Kleidon, A., Zehe, E., Ehret, U., and Scherer, U.: Thermodynamics, maximum power, and the dynamics of preferential river flow structures at the continental scale, Hydrol. Earth Syst. Sci., 17, 225–251, doi:10.5194/hess-17-225-2013, 2013. 7823
Kleidon, A., Renner, M., and Porada, P.: Estimates of the climatological land surface energy and water balance derived from maximum convective power, Hydrol. Earth Syst. Sci., 18, 2201–2218, doi:10.5194/hess-18-2201-2014, 2014. 7824
McDonnell, J., Sivapalan, M., Vaché, K., Dunn, S., Grant, G., Haggerty, R., Hinz, C., Hooper, R., Kirchner, J., Roderick, M., Selker, J., and Weiler, M.: Moving beyond heterogeneity and process complexity: a new vision for watershed hydrology, Water Resour. Res., 43, W07301, doi:10.1029/2006WR005467, 2007. 7823
Milly, P. C. D.: Climate, soil water storage, and the average annual water balance, Water Resour. Res., 30, 2143–2156, doi:10.1029/94WR00586, doi:10.1029/94WR00586, 1994. 7834
Porada, P., Kleidon, A., and Schymanski, S. J.: Entropy production of soil hydrological processes and its maximisation, Earth Syst. Dynam., 2, 179–190, doi:10.5194/esd-2-179-2011, 2011. 7823, 7824, 7827

HESSD
12, 7821–7842, 2015

Potter, N. J., Zhang, L., Milly, P. C. D., McMahon, T. A., and Jakeman, A. J.: Effects of rainfall seasonality and soil moisture capacity on mean annual water balance for Australian catchments, Water Resour. Res., 41, w06007, doi:10.1029/2004WR003697, 2005. 7834

Rinaldo, A., Rodriguez-Iturbe, I., Rigon, R., Bras, R. L., Ijjasz-Vasquez, E., and Marani, A.: Minimum energy and fractal structures of drainage networks, Water Resour. Res., 28, 2183–2195, doi:10.1029/92WR00801, 1992. 7823

Rodriguez-Iturbe, I., Rinaldo, A., Rigon, R., Bras, R. L., Ijjasz-Vasquez, E., and Marani, A.: Fractal structures as least energy patterns: The case of river networks, Geophys. Res. Lett., 19, 889–892, doi:10.1029/92GL00938, 1992. 7823

Savenije, H. H. G.: The importance of interception and why we should delete the term evapotranspiration from our vocabulary, Hydrol. Process., 18, 1507–1511, doi:10.1002/hyp.5563, 2004. 7832

Schaake, J., Cong, S., and Duan, Q.: The US MOPEX data set, IAHS-AISH P., 307, 9–28, 2006. 7832

Schaefli, B., Harman, C. J., Sivapalan, M., and Schymanski, S. J.: HESS Opinions: Hydrologic predictions in a changing environment: behavioral modeling, Hydrol. Earth Syst. Sci., 15, 635–646, doi:10.5194/hess-15-635-2011, 2011. 7823

Sivapalan, M., Blöschl, G., Zhang, L., and Vertessy, R.: Downward approach to hydrological prediction, Hydrol. Process., 17, 2101–2111, 2003. 7823

Thompson, S., Harman, C., Troch, P., Brooks, P., and Sivapalan, M.: Spatial scale dependence of ecohydrologically mediated water balance partitioning: a synthesis framework for catchment ecohydrology, Water Resour. Res., 47, W00J03, doi:10.1029/2010WR009998, 2011. 7823

van Genuchten, M. T.: A closed-form equation for predicting the hydraulic conductivity of unsaturated soils, Soil Sci. Soc. Am. J., 44, 892–898, doi:10.2136/sssaj1980.03615995004400050002x, 1980. 7827

Wang, D. and Tang, Y.: A one-parameter Budyko model for water balance captures emergent behavior in darwinian hydrologic models, Geophys. Res. Lett., 41, 4569–4577, doi:10.1002/2014GL060509, 2014. 7824

Wang, D., Zhao, J., Tang, Y., and Sivapalan, M.: A thermodynamic interpretation of Budyko and L'vovich formulations of annual water balance: proportionality hypothesis and maximum entropy production, Water Resour. Res., 51, 3007–3016, doi:10.1002/2014WR016857, 2015. 7824

HESSD
12, 7821–7842, 2015

Wang, J. and Bras, R. L.: A model of evapotranspiration based on the theory of maximum entropy production, Water Resour. Res., 47, W03521, doi:10.1029/2010WR009392, 2011. 7823

Westhoff, M. C. and Zehe, E.: Maximum entropy production: can it be used to constrain conceptual hydrological models?, Hydrol. Earth Syst. Sci., 17, 3141–3157, doi:10.5194/hess-17-3141-2013, 2013. 7823, 7824

Westhoff, M. C., Zehe, E., and Schymanski, S. J.: Importance of temporal variability for hydrological predictions based on the maximum entropy production principle, Geophys. Res. Lett., 41, 67–73, doi:10.1002/2013GL058533, 2014. 7823, 7824, 7832

Yang, H., Yang, D., Lei, Z., and Sun, F.: New analytical derivation of the mean annual water-energy balance equation, Water Resour. Res., 44, W03410, doi:10.1029/2007WR006135, 2008. 7827

Zehe, E., Blume, T., and Blöschl, G.: The principle of "maximum energy dissipation": a novel thermodynamic perspective on rapid water flow in connected soil structures, Philos. T. R. Soc. B, 365, 1377–1386, doi:10.1098/rstb.2009.0308, 2010. 7823

Zehe, E., Ehret, U., Blume, T., Kleidon, A., Scherer, U., and Westhoff, M.: A thermodynamic approach to link self-organization, preferential flow and rainfall–runoff behaviour, Hydrol. Earth Syst. Sci., 17, 4297–4322, doi:10.5194/hess-17-4297-2013, 2013. 7823, 7832

Zehe, E., Ehret, U., Pfister, L., Blume, T., Schröder, B., Westhoff, M., Jackisch, C., Schymanski, S. J., Weiler, M., Schulz, K., Allroggen, N., Tronicke, J., van Schaik, L., Dietrich, P., Scherer, U., Eccard, J., Wulfmeyer, V., and Kleidon, A.: HESS Opinions: From response units to functional units: a thermodynamic reinterpretation of the HRU concept to link spatial organization and functioning of intermediate scale catchments, Hydrol. Earth Syst. Sci., 18, 4635–4655, doi:10.5194/hess-18-4635-2014, 2014. 7823

Zhang, L., Hickel, K., Dawes, W. R., Chiew, F. H. S., Western, A. W., and Briggs, P. R.: A rational function approach for estimating mean annual evapotranspiration, Water Resour. Res., 40, w02502, doi:10.1029/2003WR002710, 2004. 7834

HESSD
12, 7821–7842, 2015

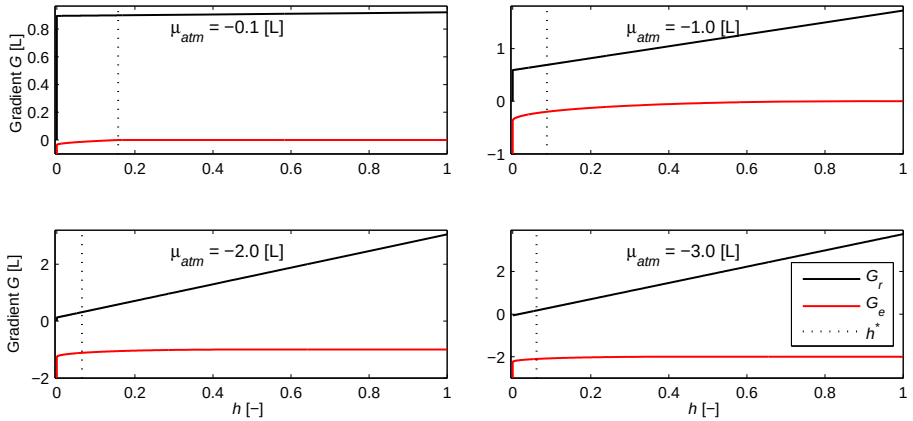

Figure 1. The gradients driving evaporation (G_e) and runoff (G_r) as a function of the relative saturation (h) for different values of μ_{atm} with $k_r = k_r^*$ and $n = 2$. At $h = 0$, the slope of the gradient G_e is vertical, while the value of G_r is set to zero to avoid runoff at zero saturation.

HESSD
12, 7821–7842, 2015

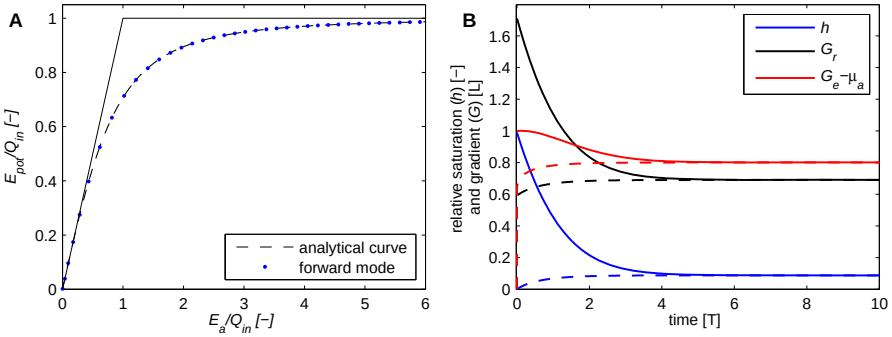

Figure 2. (a) Analytical Budyko curve (Eq. 9) and result from forward mode with constant forcing for $n = 2$ and **(b)** time evolution of relative saturation and both gradients for complete initial saturation (solid lines) and initial dry state (dashed lines). $\mu_{atm} = -1$.

HESSD
12, 7821–7842, 2015

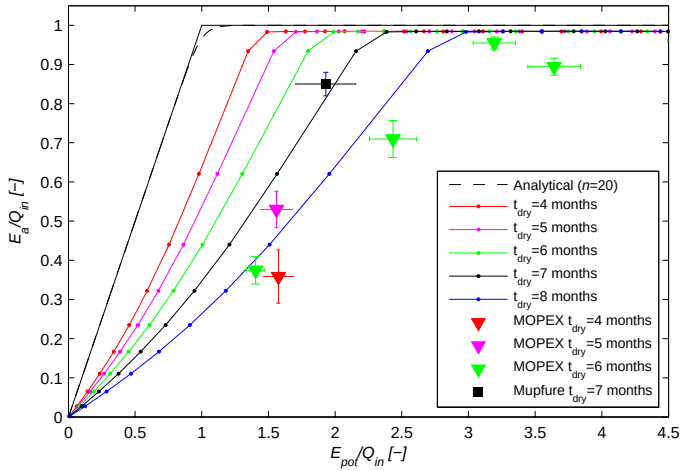

Figure 3. Sensitivity to periodic dry spells to the forward model. MOPEX catchments are filtered to have only those catchments having at least one month with a median rainfall $< 2.5\,\mathrm{mm\,month^{-1}}$ and a coefficient of variance < 0.5 for all months with a median rainfall $> 25\,\mathrm{mm\,month^{-1}}$. The final number of dry months were determined maximizing the difference between the mean monthly precipitation of the X driest months minus the mean monthly precipitation of the $1 - X$ wettest months, where $X = 1, 2 \ldots 12$. Error bars indicate one standard deviation and are determined with bootstrap sampling.

HESSD
12, 7821–7842, 2015

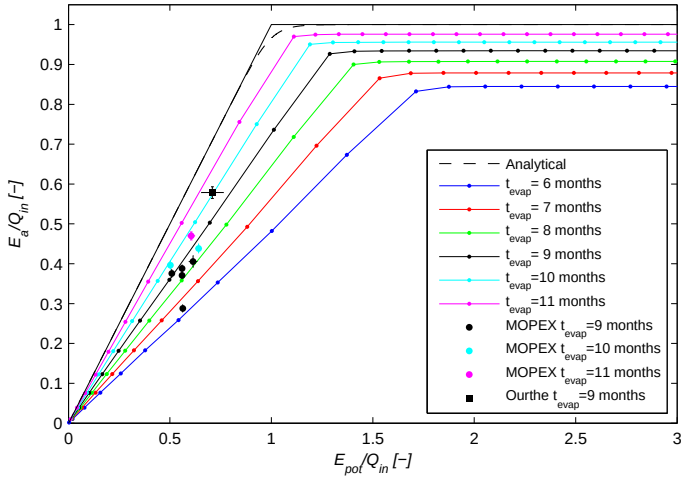

Figure 4. Sensitivity to on-off dynamics in actual evaporation to the forward model. MOPEX catchments were filtered to have only those catchments having a coefficient of variance < 0.12 for monthly median rainfall and with at least one month with a median maximum air temperature < 0 °C; a month is considered to have no actual evaporation if the monthly median maximum air temperature < 0 °C (after Devlin, 1975). Error bars indicate one standard deviation and are determined with bootstrap sampling.

HESSD
12, 7821–7842, 2015